Conformations of Trypsin-Bound Amidine Inhibitors of Blood Coagulant Factor Xa by Double REDOR NMR and MD Simulations

Lynda M. McDowell,[†] Margaret A. McCarrick,[‡] Daniel R. Studelska,[†] William J. Guilford,[‡] Damian Arnaiz,[‡] Jerry L. Dallas,[‡] David R. Light,[‡] Marc Whitlow,[‡] and Jacob Schaefer*[,†]

Department of Chemistry, Washington University, St. Louis, Missouri 63130, and Berlex Biosciences, 15049 San Pablo Avenue, Richmond, California 94804

Received February 8, 1999

Double rotational-echo double resonance (double REDOR) has been used to investigate the bound conformations of ^{13}C,^{15}N,^{19}F-labeled factor Xa inhibitors to bovine trypsin. Carbon−fluorine dipolar couplings were measured by $^{13}C\{^{19}F\}$ REDOR with natural-abundance background interferences removed by $^{13}C\{^{15}N\}$ REDOR. The conformations of the bound inhibitors were characterized by molecular dynamics (MD) simulations of binding restrained by double REDOR-determined intramolecular C−F distances. A symmetrical bisamidine inhibitor and an asymmetrical monoamidine−monoamine inhibitor of the same general shape had distinctly different conformations in the bound state. According to the MD models, these differences arise from specific interactions of the amidine and amine groups with the active-site residues of trypsin and nearby water molecules.

Introduction

Factor Xa (FXa) is a 45-kDa enzyme belonging to the serine protease class. FXa, as part of the prothrombinase complex with factor Va, phospholipids, and calcium, proteolytically converts prothrombin to thrombin in the rate-limiting step of blood coagulation.[1] Thrombin promotes clot formation by catalyzing the release of polymerizable fibrin from fibrinogen and promoting platelet aggregation. Thrombin and FXa are drug-design targets because of their important roles in thrombus formation. Recent in vivo studies demonstrate that potent FXa inhibitors are efficacious in models of both venous and arterial thrombosis without causing an increase in bleeding.[2] Several groups have identified synthetic nonpeptide compounds that selectively inhibit FXa relative to thrombin.[3] Most of these compounds exhibit only weak (about 10-fold) specificity over trypsin, a major digestive enzyme which is also a serine protease. However, a series of bisamidine inhibitors was discovered at Berlex that has high specificity for FXa versus trypsin while maintaining potency against thrombin.[3a] Knowledge of the binding modes and mechanisms of FXa specificity for these compounds could be useful in the drug-development process.

The crystal structure of the symmetrical bisamidine inhibitor ZK-805623 (**1**) bound to trypsin has been obtained at 1.8-Å resolution.[4] One phenylamidine appears to be fixed in the trypsin P1 binding site. The other phenylamidine results in weaker electron-density plots, leading to some ambiguity in the position of the phenyl group. This ambiguity is due to either dynamics or conformational heterogeneity, which suggests that in trypsin, only one end of the inhibitor is firmly anchored to the protein. The rotational-echo double resonance[5,6] (REDOR) experiments reported here were performed to determine the bound conformation of **1**, as well as that of the asymmetric monoamidine ZK-806299 (**2**), by measuring key distances between the fluorines of the central rings of **1** and **2** and the symmetrical amidino carbons of **1**, or the amidino and amino carbons of **2**. Both **1** and **2** belong to a class of compounds that selectively inhibit FXa.[3a] Compound **2** is only weakly selective for FXa as compared to trypsin, but **1** is highly selective (Table 1). Trypsin was used for these initial REDOR binding studies instead of FXa because of the much lower cost. This is the first step in a program whose goal is to understand the high FXa/trypsin selectivity of the 2,6-bis(amidinoaryloxy)pyrimidine template.

Table 1. Inhibition Constants (nM) for **1** and **2** (unlabeled) in Trypsin and FXa

compd	trypsin	FXa
1	740[a]	12[a]
2	2900[b]	1400[b]

[a] Reference 3a. [b] This work.

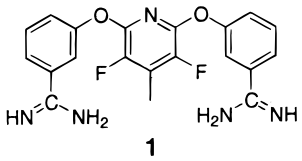

1

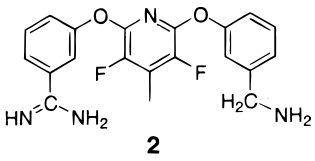

2

Experimental Methods

Synthesis and Characterization of Inhibitors. The synthesis of the labeled inhibitors is shown in Schemes 1 and 2. The symmetrical inhibitor **1** was prepared by condensing 2 equiv of labeled (^{13}C,^{15}N)cyanophenol with 4-methyl-2,3,5,6-tetrafluoropyridine to give the bisbenzonitrile intermediate **5**. Reaction of **5** with HCl gas in ethanol gave the imidate which yielded the desired bisamidine upon treatment with (^{15}N)-ammonia. Mass spectal analysis of the isolated bisamidine showed six labeled atoms had been incorporated.

[†] Washington University.
[‡] Berlex Biosciences.

10.1021/jm9900669 CCC: $18.00
Published on Web 09/03/1999

Scheme 1. Synthesis of Stable Isotope-Labeled **1**[a]

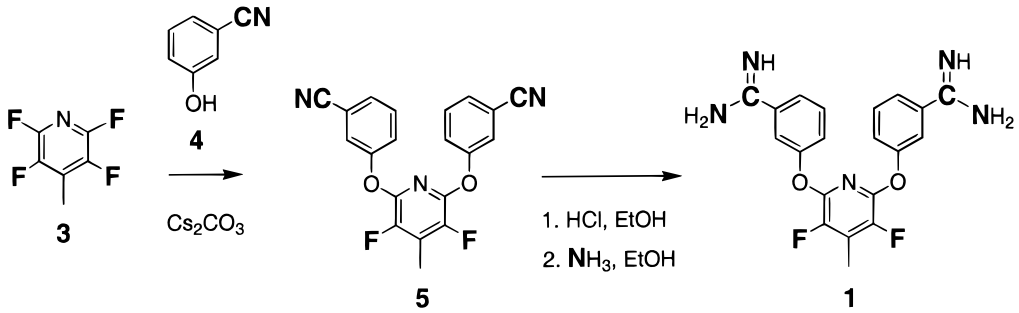

[a] ^{13}C and ^{15}N labels, as well as ^{19}F, are shown in boldface.

Scheme 2. Synthesis of Stable Isotope Labeled **2**[a]

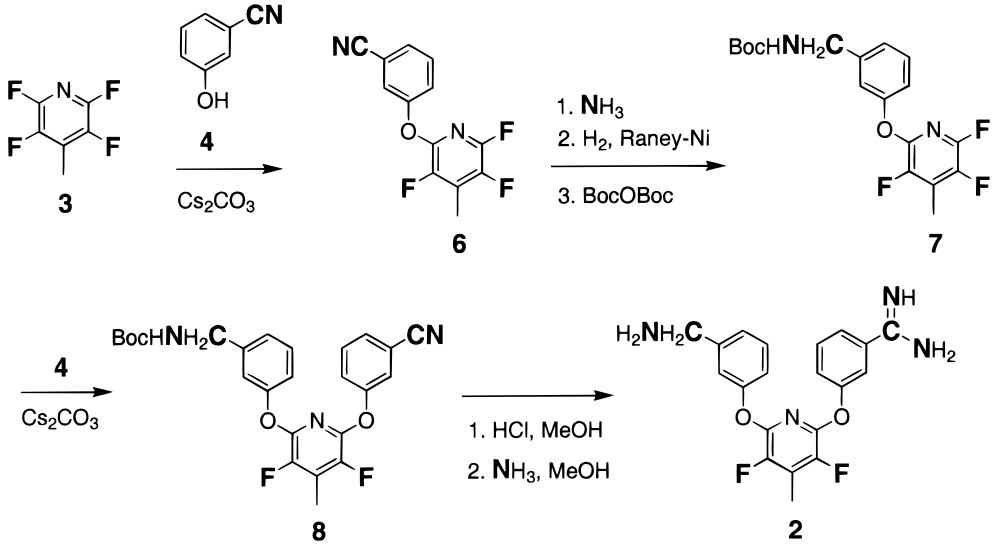

[a] ^{13}C and ^{15}N labels, as well as ^{19}F, are shown in boldface.

The unsymmetrical inhibitor **2** was prepared by condensing 1 equiv of labeled (^{13}C,^{15}N)cyanophenol with 4-methyl-2,3,5,6-tetrafluoropyridine to give the monobenzonitrile product. The nitrile group was reduced with Raney nickel, and the resulting amine was protected with a Boc protecting group. Condensation of **7** with hydroxybenzo(^{13}C,^{15}N)nitrile gave the bisaryl ether **8**. The nitrile was converted to the amidine as for the symmetrical inhibitor.

Labeled syntheses were carried out initially using unlabeled reagents and gave identical products in similar yields. Labeled reagents were obtained from Isotec, Inc. (Miamisburg, OH): (^{13}C,^{15}N)cyanophenol (99 at. % ^{13}C,^{15}N) and (^{15}N)ammonia (99.9 at. %). All of the other reagents were obtained from Aldrich. Proton and ^{13}C NMR spectra were obtained on Varian 300- and 400-MHz spectrometers, respectively. Chemical shifts are reported in parts per million downfield from tetramethylsilane. High-performance liquid chromatography (HPLC) was carried out with a Rainin HPLX system equipped with two 50-mL pump heads using a Rainin Dynamax 41.4-mm × 250-mm (preparative) column packed with 60-Å C-18 bonded silica.

2,6-Bis[(^{15}N,^{13}C-*cyano*)phenoxy]-3,5-difluoro-4-methylpyridine (5). A slurry of (^{13}C,^{15}N)cyanophenol (0.5 g, 4.1 mmol) and cesium carbonate (1.4 g, 4.4 mmol) in DMSO (20 mL) under nitrogen was stirred and heated in a 70 °C oil bath for 30 min before the addition of 4-methyl-2,3,5,6-tetrafluoropyridine (0.23 mL, 2 mmol). The reaction was stirred for 2 h at 70 °C and then allowed to cool. Mixture was poured into a mixture of ice-cold 0.1 N sodium hydroxide, methanol, and ethyl acetate. The aqueous layer was extracted with ethyl acetate. The combined organic layers were washed with 0.1 N sodium hydroxide, water (2×), and brine, dried ($MgSO_4$), treated with charcoal, filtered through Celite, and concentrated. Residue was recrystallized from ethyl acetate and hexane to give **5** (0.57 g, 78%) as a white solid: ^1H NMR ($CDCl_3$) 7.45 (m, 4H), 7.25 (m, 4H), 2.41 (m, 3H).

2,6-Bis[(^{15}N-*amino*-^{15}N-*imino*-^{13}C-*methyl*)phenoxy]-3,5-difluoro-4-methylpyridine (1). A solution of **5** (0.4 g, 1 mmol) in absolute ethanol (100 mL) was stirred at −78 °C as gaseous hydrochloride gas was added to yield a saturated solution. The reaction was sealed and allowed to stand at ambient temperature for about 20 h. Solvent was removed under reduced pressure, and the imidate intermediate was dried under high vacuum. Residue was dissolved in absolute ethanol (50 mL), placed in a pressure vessel under a nitrogen atmosphere, and cooled to −78 °C. Labeled (^{15}N)ammonia (1 L) was bubbled in. Reaction was sealed and heated at 40 °C for 2 days. Purification by preparative HPLC using a 40−50% acetonitrile in water gradient with 0.1% trifluoroacetic acid gave 140 mg of a white solid after salt exchange with 6 N hydrochloric acid: ^1H NMR (DMSO-d_6) 9.5 (m, 4H), 9.14 (m, 4H), 7.65 (m, 4H), 7.52 (m, 4H), 2.41 (m, 3H); ^{13}C NMR (DMSO-d_6) 164.2 (C-Am), 164.1 (C-Am), 163.99 (C-Am), 163.95 (C-Am), 163.81 (C-Am), 151.8 (C-1), 140.59 (C-pyr), 139.97 (C-pyr), 139.52 (C-pyr), 128.7 (C-5), 127.1 (C-3), 123.3 (C-6), 122.1 (C-4), 117.3 (C-2); MS m/e = 403 (M^+).

2-(^{13}C,^{15}N-*cyano*)Phenoxy-4-methyl-3,5,6-trifluoropyridine (6). To a solution of 4-methyl-2,3,5,6-tetrafluoropyridine (0.36 mL, 3.14 mmol), (^{13}C,^{15}N)cyanophenol (0.25 g, 2.08 mmol), and DMSO (10 mL) was added cesium carbonate (1.35 g, 4.14 mmol). The reaction mixture was stirred for 4 h and then poured into water (30 mL). The aqueous layer was extracted with dichloromethane (2 × 50 mL). The organic layers were washed with additional water (30 mL) and brine (30 mL), dried ($MgSO_4$), and concentrated. Purification by silica gel chromatography using a 10−20% ethyl acetate gradient in hexane afforded 480 mg (87%) of **6** as a white

solid: ^{1}H NMR ($CDCl_3$) 7.59−7.50 (m, 2H), 7.48−7.39 (m, 3H), 2.40 (s, 3H).

2-[3-*N*-(1,1-Dimethylethoxycarboxy)(^{15}N-*amino*-^{13}C-*methyl*)phenoxy]-4-methyl-3,5,6-trifluoropyridine (7). A solution of **6** (480 mg, 1.80 mmol) in methanol (50 mL) at −50 °C was treated with (^{15}N)ammonia (g). The solution was warmed to room temperature, and then Raney nickel (2 mL of a 50 wt % solution in water) was added. The resulting mixture was placed under hydrogen (20 psi) and shaken for 1 h. The reaction mixture was then filtered and the filtrate concentrated to afford a light oil. To a solution of the light oil and THF (10 mL) was added Boc anhydride (1.10 g, 5.0 mmol). The reaction mixture was stirred for 16 h. The THF was removed, and the resulting oil was dissolved in dichloromethane (80 mL). The organic layer was washed with water (50 mL) and brine (50 mL), dried ($MgSO_4$), and concentrated. Purification by silica gel chromatography using 4:1 hexane:ethyl acetate afforded 405 mg (61%) of **7** as a clear oil.

2-[3-(^{13}C,^{15}N-*cyano*)Phenoxy]-3,5-difluoro-6-[3-*N*-(1,1-dimethylethoxycarboxy)(^{15}N-*amino*-^{13}C-*methyl*)phenoxy]-4-methylpyridine (8). To a solution of **7** (0.40 g, 1.12 mmol), (^{13}C,^{15}N)cyanophenol (0.14 g, 1.12 mmol), and DMSO (10 mL) was added cesium carbonate (0.55 g, 1.70 mmol). The reaction mixture was warmed to 80 °C, stirred for 7 h, and then poured into water (50 mL). The aqueous layer was extracted with ethyl acetate (2 × 80 mL). The organic layers were washed with brine (50 mL), dried ($MgSO_4$), and concentrated. Purification by silica gel chromatography using 4:1 hexane:ethyl acetate afforded 268 mg (51%) of **8** as a white solid: ^{1}H NMR ($CDCl_3$) 7.50−7.25 (m, 4H), 7.15−7.05 (m, 1H), 6.98−6.90 (m, 3H), 4.90 (d, 1H), 4.30 (d, 2H), 2.40 (s, 3H), 1.70−1.38 (m, 9H).

2-[3-(^{15}N-*amino*-^{15}N-*imino*-^{13}C-*methyl*)Phenoxy]-6-[3-(^{15}N-*amino*-^{13}C-*methyl*)phenoxy]-3,5-difluoro-4-methylpyridine (2). A solution of **8** (0.26 g, 0.55 mmol), dichloromethane (2 mL), and methanol (20 mL) at −20 °C was treated with HCl (g). The reaction was warmed to room temperature and then allowed to stand for 16 h. The reaction was concentrated to afford an oil. The oil was dissolved in methanol (20 mL) and cooled to −50 °C. The solution was then treated with (^{15}N)ammonia (g). The reaction solution was sealed and warmed to 50 °C, stirred for 16 h, and then concentrated. Purification by HPLC using a 20−60% acetonitrile in water gradient with 0.1% trifluoroacetic acid afforded 120 mg (74%) of **2** as the trifluoroacetate salt: ^{1}H NMR (DMSO-d_6) 9.40 (d, 2H), 9.10 (d, 2H), 8.30 (br s, 1H), 8.10 (br s, 1H), 7.80−7.50 (m, 4H), 7.40−7.30 (m, 1H), 7.25−7.10 (m, 3H), 4.00 (d, 2H), 2.40 (s, 3H); MS *m*/*z* 389 (M^+). Anal. Calcd for $(C_{20}H_{18}F_2N_4O_2 \cdot 2CF_3CO_2H \cdot H_2O)$ C, H, F, N.

Solid-State NMR Sample Preparation. Trypsin (3× crystallized, TPCK-treated, dialyzed against 1 mM HCl, and lyophilized) was purchased from Worthington Biochemical Corp. (Freehold, NJ). Residual chloride was removed from the trypsin by several cycles of ultrafiltration in 20 mM formate buffer, pH 3.9. The concentrated enzyme solution (100 mg in 5−6 mL) was then diluted to 30−35 mL with 5 mM HEPES (pH 8), 12 mM trehalose, 0.6, 2, or 4 mM hemicalcium salt of cyclamic acid, and 0.05% or 0.1% PEG-8000 before inhibitor addition. An equimolar ratio of **1** was added; the sample was frozen and lyophilized. Many lyophilization conditions were tested to achieve a porous cake in the final state, including use of low temperatures (−30 °C) and addition of Dextran (20 mg each, MW 81.5 and 488 kDa). While the appearance of the lyophilized cake varied, the REDOR-determined distances were the same for all samples complexed with **1** employed in this study. The trypsin/**2** complexes were made as described above, using Dextran and low-temperature lyophilization.

REDOR and Double REDOR. REDOR dephasing[5] is measured by $\Delta S/S_0$, where ΔS (the REDOR difference) equals $S_0 - S$, and S and S_0 are the observed echo intensities with and without dephasing pulses, respectively. The REDOR dephasing for a heteronuclear pair is proportional to the third power of the inverse distance between the spins and hence is a direct measure of interatomic distances.[5] Double REDOR consists of two separate REDOR experiments performed sequentially.[6] For trypsin complexes of labeled **1** and **2**, ^{13}C-{^{15}N} REDOR dephasing was used to remove interferences from the natural-abundance ^{13}C background and ^{13}C{^{19}F} REDOR dephasing was used to measure distances. (The nucleus outside the curly bracket in this notation is the observed spin, and the nucleus inside the bracket is the dephasing spin.) Double REDOR is preferred to transferred-echo double resonance (TEDOR) for background suppression[7] if there are multiple pairs of spins with different C−N couplings because it is impossible to optimize a TEDOR coherence transfer for all pairs at the same time. This was the situation for trypsin/**2**. The 50.3-MHz ^{13}C{^{15}N or ^{19}F} double REDOR experiments were performed using either a single ^{13}C refocusing 10-μs π pulse with all remaining 10-μs π pulses under *xy*-8 phase alternation[8] on the ^{15}N or ^{19}F dephasing channel[6] or equal numbers of refocusing and dephasing pulses and *xy*-8 phase alternation on both channels.[7] The initial carbon magnetization was generated by a 2-ms matched cross-polarization transfer from the protons. A 2-s repetition period was used throughout. Details of the pulse sequence, probe, and spectrometer for double REDOR have been discussed elsewhere.[6]

Dipolar Rotational Spin−Echo NMR. Nitrogen−proton dipolar interactions were characterized by a version of dipolar rotational spin−echo (DRSE) 30.4-MHz ^{15}N NMR extended over two rotor cycles.[9] This is a two-dimensional experiment in which, during the additional time dimension, nitrogen magnetization is allowed to evolve under the influence of ^{1}H−^{15}N coupling while ^{1}H−^{1}H coupling is suppressed by homonuclear multiple-pulse semiwindowless MREV-8 decoupling.[10] The cycle time for the homonuclear decoupling pulse sequence was 33.6 μs, resulting in decoupling of proton−proton interactions as large as 60 kHz. Sixteen MREV-8 cycles or loops fit exactly into two rotor periods with magic-angle spinning at 3720 Hz. The ^{15}N S/S_0 (as a function of the number of MREV loops) for a direct N−H bond is a monitor of the presence of large-amplitude molecular motions faster than 10 kHz at 267 K (the temperature of the experiment). Such motions reduce the dipolar coupling and increase S/S_0 relative to those observed for rigid materials.[11] The $^{15}NH_2$ amide nitrogen of crystalline labeled asparagine and the $^{15}NH_3^+$ amine nitrogen of crystalline labeled alanine·HCl were used as rigid DRSE models for the cationic amidine and amine nitrogens, respectively, of trypsin/**2**.

Computational Methods. (A) Protein Model. The crystal structure of bovine trypsin complexed with the symmetrical inhibitor **1** was used as a starting point for molecular modeling studies.[4] Where more than one side chain position was given, only the A position was retained. Crystallographic waters and ions were removed. The AMBER 4.1 program was used for molecular dynamics (MD) simulations and energy minimization of the protein/inhibitor complexes.[12] Hydrogen atoms, chloride counterions, and a 20-Å cap of water molecules centered on **1** were added to the crystal coordinates. Trypsin residues with at least one heavy atom within 8 Å of the inhibitor were allowed to move during energy minimization and MD simulations. The following residues were in the moving set (the chymotrypsin-numbering scheme was used throughout): 57, 96−99, 172−176, 189−192, 194−195, 213−221A, and 224−228. Half-harmonic restraints with a force constant of 10 kcal/(mol·Å^2) were applied to the water molecules to prevent evaporation. The SHAKE algorithm was used to constrain all bond lengths to their equilibrium values during MD.[13] A time step of 2 fs was used. The system was kept at a constant temperature of 298 K using the Berendsen algorithm with a coupling constant of 0.2 ps for the solute and 0.1 ps for the water cap.[14]

(B) Inhibitor Models. The AMBER 4.1 force field was used, with some additional parameters to describe the inhibitors.[15] These parameters had been developed for a thermodynamic study of related inhibitors complexed with FXa. The new parameters used are listed in Table 2. Partial charge models were derived for the inhibitors by fitting to the electrostatic potentials from ab initio 6-31G*//3-21G optimized

Table 2. AMBER Parameters and Sources

atom type	ϵ	R^*	source
CZ	0.0860	1.908	CA

bond type	k_s	R_0	source
C−OS	450	1.364	C−OH
CA−F	450	1.320	ab intio, 3,5-difluoro-2,6-dimethoxy-4-methylpyridine
CA−CZ	469	1.470	ab initio, benzamidine
CZ−N2	427	1.321	CA−N2

angle type	k_b	ϑ_0	source
CA−C−OS	70	120	CA−C−OH
C−OS−C	60	120	CT−OS−CT (k) and ab initio (ϑ)
NC−C−OS	70	119.3	NC−CA−N2
C−NC−C	70	120.5	C−NC−CA
C−CA−F	70	120	CA−CA−CT, CA−C−OH
CA−C−NC	70	121.5	CM−CA−NC
CA−CA−F	70	120	CA−CA−CT, CA−C−OH
CA−CA−CZ	63	120	CA−CA−CA
CA−CZ−N2	63	120	CA−CA−CA
N2−CZ−N2	70	120	N2−CA−N2
CZ−N2−H	35	120	CA−N2−H

dihedral angle type	$V/2$	phase offset	periodicity	source
X−C−OS−X	1	180	2	ab initio, anisole
NC−C−OS−C	2	180	2	ab initio, 2-methoxypyridine
NC−C−OS−C	0.5	180	1	ab initio, 2-methoxypyridine
CA−CA−CZ−N2	0.9125	180	2	ab initio, benzamidine
CA−CA−CZ−N2	0.25	0	4	ab initio, benzamidine
X−CZ−N2−X	2.4	180	2	X−CA−N2−X

improper dihedral type	$V/2$	phase offset	periodicity	source
X−X−CZ−N2	10.5	180	2	X−X−CA−N2
X−X−C−OS	1.1	180	2	X−X−C−OH

structures.[16] The charge fitting was performed on the fragments 3,5-difluoro-2,6-dimethoxy-4-methylpyridine, 3-amidinoanisole, and 3-(aminomethyl)anisole. The amidine and amine groups were modeled as cations.

(C) MD of Protein/Ligand Complexes. The inhibitors were modeled into the active site of trypsin using the crystal coordinates of **1** from the trypsin complex as a starting point. For the asymmetric inhibitor, the phenylamidine was modeled in the P1 pocket (consistent with the observed ^{13}C chemical shift, cf below), while the benzylamine was modeled in the P4 pocket defined by Trp 215, Gln 175, and Leu 99.[17] MD was performed for 1 ns with a time step of 0.002 ps with no restraints on the C−F distances ("unrestrained MD"). Additional MD simulations were performed with C−F distance restraints determined from the REDOR data ("restrained MD"). Restrained MD simulations were performed in 50-ps increments with the force constants on the restraints increasing linearly at each time step from an initial value of 0 to a final value of 100 kcal/(mol·Å^2). The resulting models were subjected to conjugate gradient minimization for 3000 steps. The MD coordinates were saved every 5 ps for inspection. The final structures after energy minimization were used to construct a theoretical REDOR curve,[18] which was then compared with the experimental dephasing. The distance restraints for the next MD iteration were estimated from these calculated REDOR curves. The $^{13}C\{^{19}F\}$ REDOR dephasing for both inhibitor complexes depends on two $^{13}C-^{19}F$ dipolar couplings[19] because there are two fluorine atoms on the central pyridine ring. The distal fluorines can be neglected only if they are significantly farther away than the proximal fluorines, which is not the situation for the trypsin complexes of **1** and **2**. Simulations for each complex required three cycles of MD and REDOR curve fitting to reach good agreement with the data. Several simulations were performed during each iteration with different initial inhibitor conformations to search for multiple potential binding modes. Graphical presentations of the models were made using the Cerius^2 molecular modeling system (Molecular Simulations, Inc.).

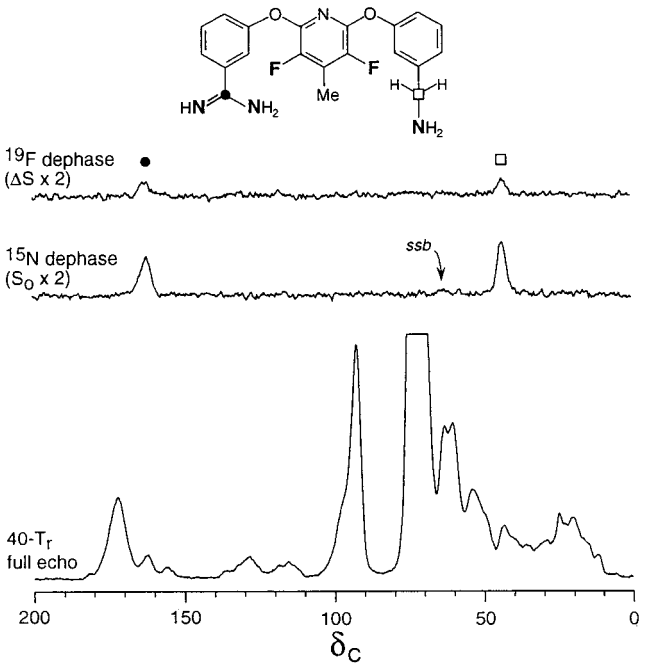

Figure 1. 50.3-MHz $^{13}C\{^{15}N$ or $^{19}F\}$ REDOR spectra of **2** bound to bovine trypsin after 40 rotor cycles of dipolar evolution with magic-angle spinning at 5 kHz. The position of the amidine ^{13}C label in the inhibitor is shown by a solid circle and that of the amine ^{13}C label by an open square. The labeled nitrogens are in boldface. REDOR dephasing by ^{15}N generates a background-free ^{13}C NMR difference spectrum (middle). REDOR dephasing by ^{19}F generates a difference spectrum (top) whose intensities as a function of dipolar evolution can be interpreted quantitatively in terms of the positions of the two fluorines of the central ring. For this determination, the $^{13}C\{^{15}N\}$ REDOR difference spectrum is S_0 and the $^{13}C\{^{19}F\}$ REDOR difference spectrum is ΔS. The determination resulted from the accumulation of 135 000 scans for each of four spectra: S_0, ^{15}N dephase, S_0, ^{19}F dephase.

Table 3. Dipolar Rotational Spin−Echo $^{15}N\{^1H\}$ Intensities for Trypsin/**1**, Trypsin/**2**, L-[4-^{15}N]Asn, and L-[^{15}N]Ala

MREV loop no.	S/S_0 amidine trypsin/**1**	amidine trypsin/**2**	amide Asn	amine trypsin/**2**	amine Ala
0	1.00	1.00	1.00	1.00	1.00
1	0.62	0.65	0.61	0.88	0.90
2	0.14	0.16	0.12	0.80	0.74
3	0.04	0.05	0.03	0.71	0.64
4	0.05	0.03	0.05	0.63	0.60

Results and Discussion

Line Assignments and REDOR Dephasing. The 50.3-MHz $^{13}C\{^{15}N$ or $^{19}F\}$ REDOR spectra of the trypsin complexes of **1** and **2** are straightforward to interpret. The ^{15}N labels allow a clean separation of labeled ^{13}C signals from the natural-abundance ^{13}C background (Figures 1 and 2, middle). The shift of the amidine carbon peak of trypsin/**2** (Figure 1) matches that of the high-field member of the pair of amidine carbon peaks of trypsin/**1** (Figure 2, inset, top left). On the basis of the intensities of ^{13}C chemical shift sidebands and the extent of the $^{13}C\{^{15}N\}$ REDOR dephasing (Figures 1 and

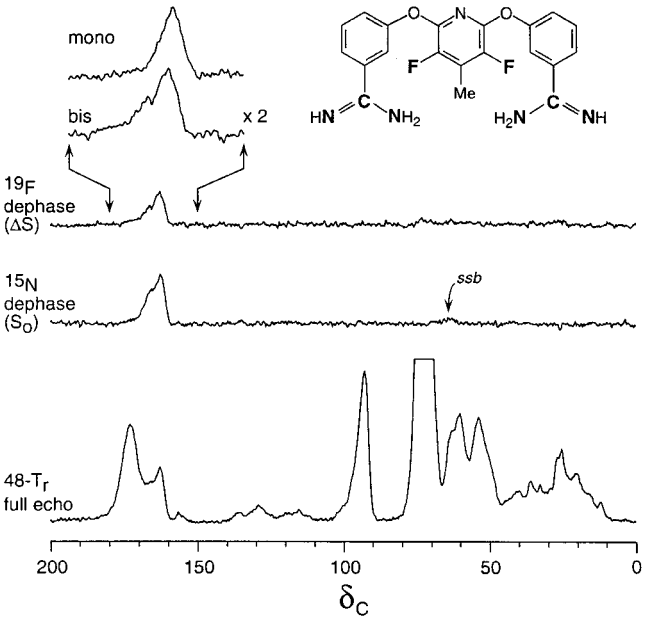

Figure 2. 50.3-MHz ^{13}C{^{15}N or ^{19}F} REDOR spectra of **1** bound to bovine trypsin after 48 rotor cycles of dipolar evolution with magic-angle spinning at 5 kHz. The labeled carbons and nitrogens are in boldface. REDOR dephasing by ^{15}N generates a background-free ^{13}C NMR spectrum (middle). The two amidine carbon resonances differ slightly in both shift position (162 and 165 ppm) and width. REDOR dephasing by ^{19}F generates a difference spectrum (top) which shows that both amidine carbon labels are near a fluorine label. The ΔS for the 162-ppm peak is larger than that of the 165-ppm peak. The chemical shift of the amidine carbon peak of trypsin/**2** matches that of the 162-ppm peak of trypsin/**1** (inset, top left). A total of 40 960 scans were accumulated for each of the four double REDOR spectra.

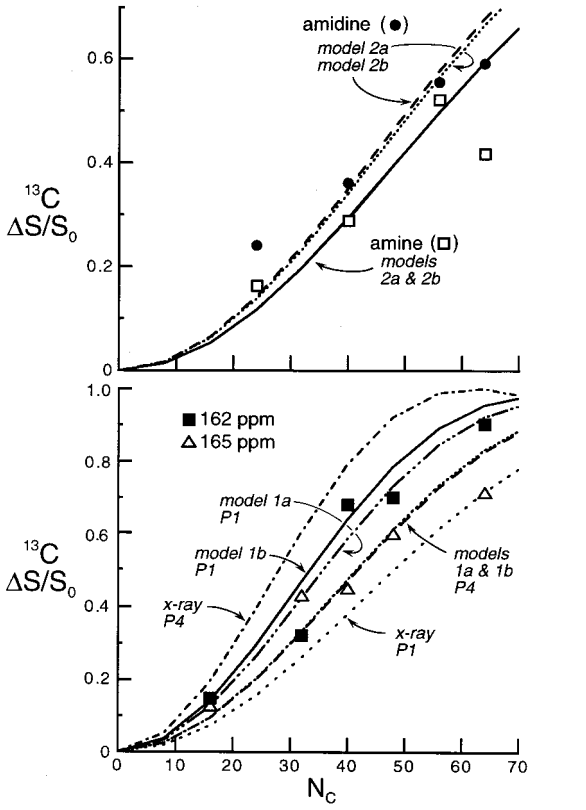

Figure 3. ^{13}C{^{19}F} REDOR dephasing ($\Delta S/S_0$) for trypsin/**1** (bottom) and trypsin/**2** (top). The dotted and solid lines represent calculated dephasing for various models (Figures 4 and 5), and the open and closed symbols represent the experimental dephasing. Determination of the dephasing for trypsin/**1** required spectral deconvolution of the overlapping amidine carbon REDOR difference peaks at 162 and 165 ppm (Figure 2).

2), as well as the full ^{15}N-^{1}H dipolar dephasing (Table 3), we see no indication of large-amplitude motions within the binding sites for either amidine or amine moieties. Thus, we associate the increased width of the 165-ppm amidine carbon peak of trypsin/**1** (Figure 2, middle) to conformational heterogeneity and a distribution of isotropic peaks, not dynamics. This hetereogeneity is consistent with the missing electron density in the X-ray structure of trypsin/**1** at the P4 binding site. We therefore assign the 162-ppm amidine carbon shift for complexes of both **1** and **2** to the more ordered, homogeneous P1 trypsin binding site.

The ^{13}C{^{19}F} REDOR dephasing ($\Delta S/S_0$) for trypsin/**1** (Figure 3, bottom) is generally greater than the dephasing for trypsin/**2** (Figure 3, top). For example, the dephasing of the 162-ppm peak of trypsin/**1** (P1 site) after 64 rotor cycles is almost 0.9, whereas that for trypsin/**2** is less than 0.6. The dephasing at the P1 site for complexes of both **1** and **2** exceeds the corresponding dephasing at the P4 site.

Modeling of the Asymmetric Inhibitor in Trypsin. MD calculations *without* REDOR restraints resulted in a model of trypsin/**2** which had a strong preference for an unsymmetrical, extended binding conformation with an amidine C−F distance of around 7.5 Å and a shorter methylamine C−F distance of around 5−7 Å. These distances are not consistent with the REDOR data, which indicate a relatively symmetrical structure with similar C−F distances. The phenylamidine moiety of **2** made the same contacts in the P1 pocket of the unrestrained MD model as is seen in the trypsin/**1** crystal structure, while the phenylamine moiety was either solvent-exposed or packed against Leu 99. The amino group itself was solvent-exposed and made no direct protein contacts during the entire MD simulation.

MD calculations *with* REDOR restraints on the C−F distances were performed in an attempt to obtain a more complete description of the conformation of **2** in the environment of the trypsin active site. The restraint for the initial MD simulation was estimated from the experimental REDOR dephasing assuming a single C−F distance (the proximal C−F distance only). In addition, the distances between the amidino hydrogens and the carboxyl oxygens of Asp 189 were restrained to 1.8 Å to prevent this important salt bridge from breaking during the initial simulation. The strength of the C−F distance restraint was gradually increased from 0 to 100 kcal/mol·Å^2 during the simulation . This was done to allow the compound to find a favorable binding mode before fixing the C−F distance. The energies of the resulting structures were minimized, and the two proximal and two distal C−F distances were used to predict a new theoretical REDOR curve. After a few iterations of this procedure, two models emerged (Figure 4), both of which predicted dephasing that was consistent with experiment (Figure 3, top).

For the P1 site, model 2a has amidine proximal and distal C−F distances of 7.3 and 9.8 Å, respectively, while model 2b has 7.4 and 9.7 Å. For the P4 site, model 2a

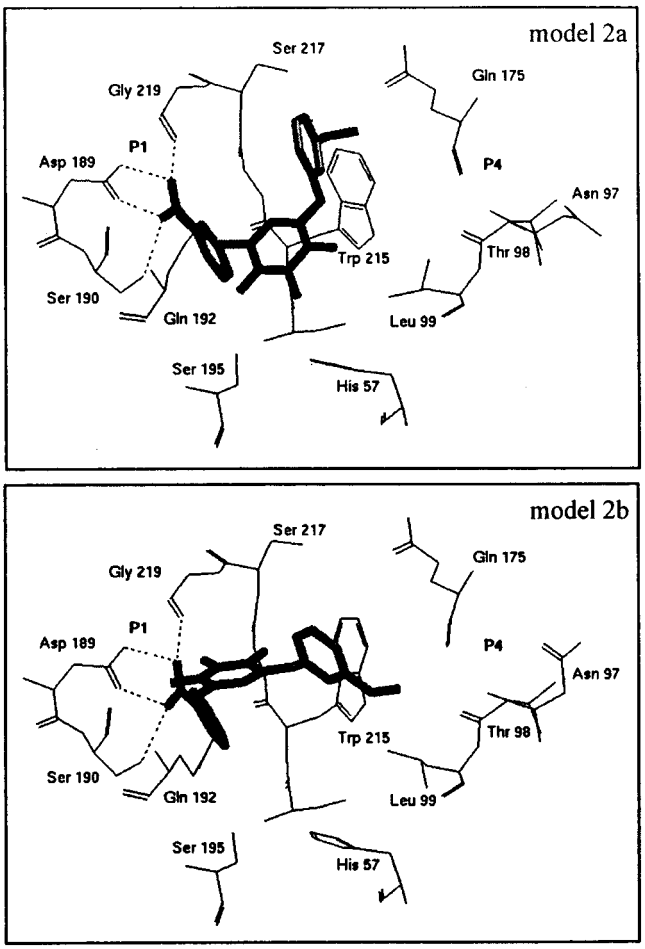

Figure 4. Two molecular models of the binding sites of trypsin containing **2**. The conformation of the inhibitor was the result of MD simulations restrained by the C−F REDOR dipolar couplings and distances from Figure 3 (top). The starting coordinates of trypsin for both models were based on the crystal structure of Whitlow et al.,[4] in which the ligand was **1**. Hydrogen bonds are indicated by dashed lines. Predicted dephasing is shown for both models in Figure 3 (top) as solid and dashed lines.

has amine proximal and distal C−F distances of 7.6 and 9.8 Å, while model 2b has 7.7 and 9.4 Å. Consideration of the distal C−F interaction shifts the theoretical REDOR curves upward (more dephasing), so that the proximal C−F distances are longer than would be predicted without including the dephasing of the distal fluorines. Therefore, it is important to consider the longer distances in addition to the nearer C−F distances to obtain accurate results. Model 2a places the amino group of the inhibitor 4.0 Å away from the hydroxy group of Ser 217 and the amido oxygen of Gln 175, with water-mediated hydrogen bonds. The hydrophobic portion of the phenylamine packs against Gly 216 and Trp 215 in this model. Model 2b places the amino group 4.8 Å from the backbone carbonyl oxygen of Asn 97 and 5.3 Å from the carbonyl oxygen of Ser 96, again with water-mediated hydrogen bonds. In this conformation, the hydrophobic portion of the phenylamine packs against Leu 99, Gly 216, and Trp 215. We do not believe that multiple conformations are necessarily present for trypsin/**2**, only that at least two conformations are consistent with the REDOR restraints.

Modeling of the Symmetric Inhibitor in Trypsin. The 162-ppm peak in trypsin/**1** (Figure 2, middle) is narrower and faster dephasing (Figure 3, bottom) than the 165-ppm peak, which means that the shorter C−F distance in trypsin/**1** is necessarily associated with the amidine carbon in the more highly ordered P1 binding site. The theoretical REDOR dephasing for a single C−F coupling indicated that both phenylamidine C−F distances were less than 7 Å, shorter than the distances for trypsin/**2**. After several iterations of restrained MD and recalculation of the theoretical REDOR dephasing, the proximal and distal distances for the resulting structure (model 1a in Figure 5) are 6.5 and 9.0 Å, respectively, for the P1 site and 6.8 and 10.0 Å, respectively, for the P4 site.

All of the preceding MD simulations used the crystal coordinates of the trypsin/**1** complex as a starting point; as a result, the simulations could be biased toward the conformation found in the crystal structure. To test for this potential bias, a thorough conformational search of **1** was undertaken. Distance geometry calculations were performed with DGEOM95[20] to generate initial conformations of free **1** consistent with the REDOR distance restraints. A total of 141 conformations were saved with the number of trials set to 100 and the rmsd rejection threshold set to 1.0 Å. These were docked into the P1 pocket of trypsin and visually inspected. Structures with obvious major steric clashes were removed, leaving 41 docked structures with no or only minor steric problems. These structures were then subjected to 500 steps of restrained minimization with AMBER using a soft repulsion term to reduce the worst contacts, followed by 3000 steps of restrained minimization of the inhibitor and nearby active-site residues using a standard Lennard−Jones interaction. The structures having the lowest interaction energies were then analyzed for their agreement with REDOR results. Only one low-energy structure was found to be consistent with experiment, and this is identified as model 1b in Figure 5. The proximal and distal distances for model 1b are 6.5 and 8.1 Å, respectively for the P1 site and 6.8 and 10.2 Å, respectively, for the P4 site. The calculated REDOR dephasing for model 1b is shown in Figure 3 (bottom).

Both REDOR models 1a and 1b resemble the X-ray structure in many respects; however, the placement of the P4 phenylamidine in model 1a does not overlap well with the crystal structure, and the placement of the pyridine ring of model 1b differs significantly from that of the X-ray structure (Figure 5). Of course, these are the portions of the crystal structure that are not well-defined. Both REDOR models of the bound ligand are more compact than that of the crystal structure. REDOR dephasing calculated using the X-ray coordinates directly is in poor agreement with experiment (Figure 3, bottom, dashed lines).

For model 1a, one phenylamidine binds in P1, as expected based on the crystal structure of trypsin with benzamidine itself, while the second phenylamidine binds in the P4 pocket with its amidine nitrogens oriented toward the backbone carbonyl oxygens of Asn 79 and Thr 80. The carbonyl groups of these residues form an electronegative region in the P4 site, where inhibitors with cationic groups have been observed.[4] Interestingly, a simple energy minimization of the solvated trypsin/**1** crystal structure coordinates shifted the conformation of **1** so that it forms two hydrogen

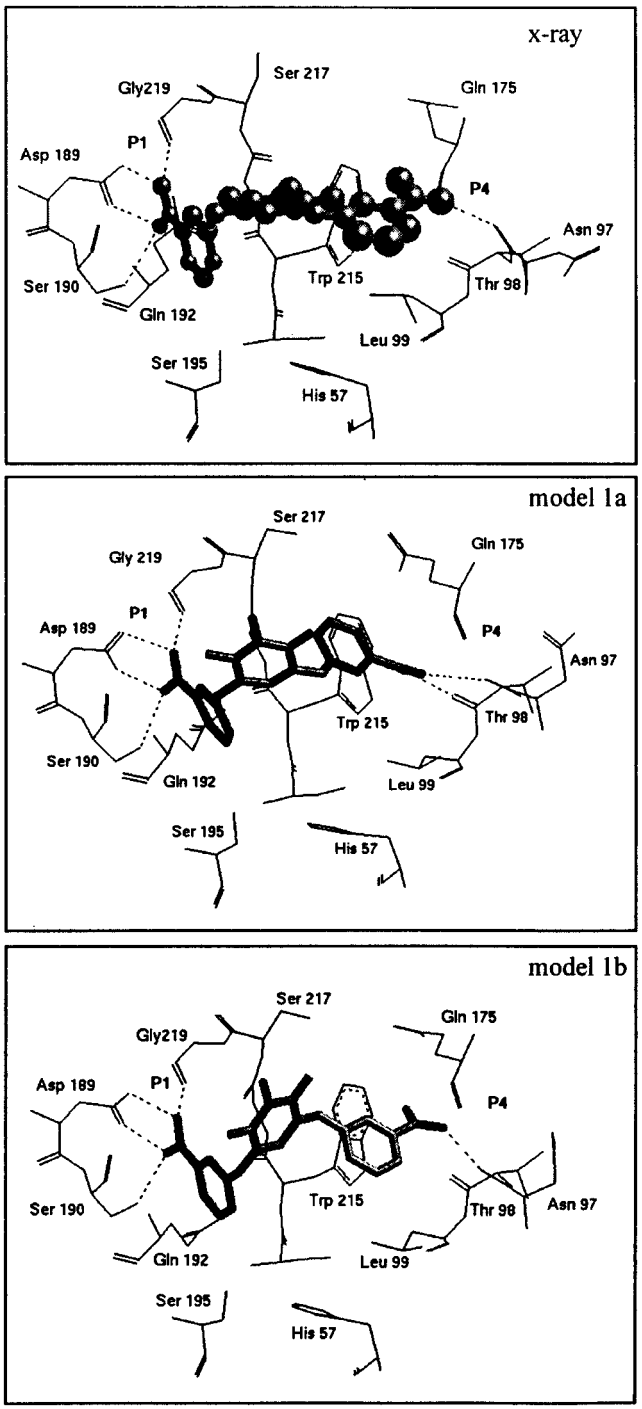

Figure 5. Molecular models of the binding sites of trypsin containing **1**. The conformation of the inhibitor in the X-ray model (top) is based on the crystal structure of Whitlow et al.[4] Uncertainties in the coordinates are shown by the sizes of the thermal ellipsoids. The conformation of the inhibitor in the REDOR model 1a (middle) was the result of MD simulations restrained by the C−F REDOR dipolar couplings and distances from Figure 3 (bottom). The starting coordinates for model 1a were taken from the crystal structure. Model 1b was determined from distance-geometry calculations starting with initial conformations of the ligand consistent with the REDOR distance restraints. Hydrogen bonds are indicated by dashed lines. Predicted dephasings for the REDOR and X-ray models are shown in Figure 3 (bottom) as solid and long-dashed lines and as short-dashed and dash−dot lines, respectively.

bonds to Asn 79 and Thr 80, consistent with the hydrogen bonding of the REDOR model 1a. According to molecular mechanics calculations of the electrostatic potential at the surfaces of trypsin and FXa, this electronegative region is even more pronounced in FXa than in trypsin. This may explain the selectivity of bisamidine inhibitors such as **1** for FXa. The hydrophobic portion of the P4 phenylamidine makes contacts with Trp 215, Gly 216, and Leu 99. The REDOR model 1a has the phenylamidine group in the P4 site rotated so that the main hydrophobic contact is with Trp 215, whereas the main contact in the crystal structure is with Leu 99. The amidine group in the REDOR model structure makes two hydrogen bonds to Asn 97 and Thr 98, whereas this group in the crystal structure has only one hydrogen bond to Asn 97.

For model 1b, the distal phenylamidine overlaps well with the crystal coordinates, making the same hydrogen bond with the carbonyl oxygen of Asn 97. Although, model 1b shows better agreement with the crystal structure than model 1a in the distal phenylamidine region, model 1b agrees better in its placement of the pyridine ring. (A structure identical to model 1b could also be found by simply energy minimizing the crystal structure coordinates with REDOR restraints.) These results indicate that a thorough conformational search can often be helpful in identifying structures which are consistent with experiment. Nevertheless, it is still difficult to get complete sampling of conformations; for example, no structures closely resembling model 1a were found using distance geometry calculations alone. A similar conformational search for **2** did not reveal any additional low-energy binding orientations that were consistent with the REDOR experimental data.

Unlike the situation for trypsin/**2**, we believe that multiple conformations are present for trypsin/**1**. This conclusion is based on the differing widths for the amidine carbon resonances (Figure 2), even though no large-amplitude motions can be detected in the matrix-stabilized complexes (Table 3). Presumably, the dynamics associated with multiple conformations have been clamped in the solid state. Because C−F distances predicted by REDOR models 1a and 1b for trypsin/**1** are so similar, the presence of multiple conformations of these types does not affect the predicted REDOR dephasing. In general, this is not the situation. Multiple conformations reduce the REDOR accuracy because the fitting of experimental and calculated dephasing must be weighted by the r_{CF}^{-3} dependence of the C−F dipolar interaction in addition to the conformer populations. We cannot rule out the possibility that conformations of trypsin/**1** with longer C−F distances than those of models 1a and 1b are also present.

Comparisons of Asymmetric and Symmetric Models. FXa inhibitors **1** and **2** show distinct differences in their binding modes despite similar shapes (Figures 4 and 5). Both C−F distances of bound **2** are longer than the corresponding C−F distances of **1**, leading to the prediction of a more extended structure for the inhibitor in trypsin/**2**. Nevertheless, the overall arrangement of both bound inhibitors is compact, with the two phenyl groups relatively close to each other. This contrasts with the extended conformation seen in trypsin crystal structures of related compounds.[4] Although the benzyl moiety of **2** packs against the protein (hydrophobic contacts are made with Trp 215 and Gly 216), the amino group remains solvated by a layer of

water molecules in the conformations of both of the models of Figure 4. This means that the phenylamino group of **2** has relatively few contacts with the protein in the P4 site, while the phenylamidine of **1** makes direct hydrogen bonds to Asn 97 and Thr 98 in the electronegative region of the P4 binding site. This arrangement may explain the much higher affinity for trypsin of **1** relative to **2**. Finally, the modeling shows that the pyridine rings of both **1** and **2** make contacts with Gln 192 but are otherwise solvent-exposed. This is consistent with the fact that substitution at the 4-position on this ring has little effect on trypsin binding affinity.[3]

The restrained MD method that was used to describe the binding of inhibitors **1** and **2** in trypsin is not an exhaustive method for searching conformational space or potential binding modes. MD trajectories tend to stay in low-energy regions, and they are limited in their ability to cross energy barriers to find new low-energy regions. The starting coordinates of the trypsin/**1** crystal structure may produce a bias toward binding modes that span the P1 and P4 sites. In fact, distance geometry calculations, followed by docking and restrained energy minimization, resulted in an additional model that was not found with MD. Other conformations and binding modes could exist which are also consistent with the experimental restraints. Nevertheless, the P1/P4 binding mode has been seen repeatedly in crystal structures of trypsin complexed with dibasic inhibitors.[4,21]

The REDOR data led to the identification of conformations that were not predicted using protein−ligand docking or unrestrained MD. The REDOR structures are more compact and more symmetrical. (Coordinates of the four model structures bound in trypsin have been deposited in the Brookhaven Protein Data Bank with identification codes 1cu7 for trypsin/**2** (both models), 1cu8 for trypsin/**1** (model 1a), and 1cu9 for trypsin/**1** (model 1b).) Thus, the REDOR experiments provided critical distance restraints that revealed a different binding mode for amidines than amines in otherwise identical dibasic inhibitors. In future work, we plan to obtain REDOR $^{13}C-^{19}F$ distance information for inhibitors **1** and **2** in FXa, which we believe may help to explain the high FXa/trypsin selectivity of the 2,6-bis-(amidinophenoxy)pyridines.

Acknowledgment. This work was supported, in part, by NIH Grant GM40634 (J.S.). The authors thank Amy Liang (Berlex) for providing trypsin binding data for unlabeled **2** and Marc Adler (Berlex) for helpful discussions.

References

(1) The blood coagulation cascade is described in several review articles, for example: (a) Mann, K. G.; Nesheim, M. E.; Church, W. R.; Haley, P.; Krishnaswamy, S. Surface-dependent Reactions of the Vitamin K-dependent Enzyme Complexes. *Blood* **1990**, *76*, 1−16. (b) Davie, E. W.; Fujikawa, K.; Kisiel, W. The Coagulation Cascade: Initiation, Maintenance, and Regulation. *Biochemistry* **1991**, *30*, 10363−10370.

(2) (a) Sullivan, M.; Morser, J.; Light, D.; Guilford, W.; Vergona, R.; Hermann, M.; White, K.; Phillips, G.; Davey, D.; Morrissey, M.; Fredrich, M.; Baldus, B. The Efficacy and Safety of BX-8107834, a Potent, Selective Factor Xa Inhibitor, in Animal Models. *FASEB J.* **1998**, *12*, A719. (b) Baum, P.; Light, D.; Verhallen, P.; Sullivan, M.; Eisenberg, P.; Abendschein, D. Antithrombotic Effects of a Novel Antagonist of Factor Xa. *Circulation* **1998**, *98*, I-800.

(3) (a) Phillips, G. B.; Buckman, B. O.; Davey, D. D.; Eagen, K. A.; Guilford, W. J.; Hinchman, J.; Ho, E.; Koovakkat, S.; Liang, A.; Light, D. R.; Mohan, R.; Ng, H. P.; Post, J. M.; Shaw, K. J.; Smith, D.; Subramanyam, B.; Sullivan, M. E.; Trinh, L.; Vergona, R.; Walters, J.; White, K.; Whitlow, M.; Wu, S.; Xu, W.; Morrissey, M. M. Discovery of N-[2-[5-[Amino(imino)methyl]-2-hydroxyphenoxy]-3,5-difluoro-6-[3-(4,5-dihydro-1-methyl-1H-imidazol-2-yl)phenoxy]pyridin-4-yl]-*N*-methylglycine (ZK-807834): A Potent, Selective, and Orally Active Inhibitor of the Blood Coagulation Enzyme Factor Xa. *J. Med. Chem.* **1998**, *41*, 3557−3562. (b) Sturzebecher, J.; Sturzebecher, U.; Vieweg, H.; Wagner, G.; Hauptmann, J.; Markwardt, F. Synthetic Inhibitors of Bovine Factor Xa and Thrombin. Comparison of their Anticoagulant Efficiency. *Thromb. Res.* **1989**, *54*, 245−252. (c) Hara, T.; Yokoyama, A.; Ishihara, H.; Yokoyama, Y.; Nagahara, T.; Iwamoto, M. DX-9065a, A New Synthetic, Potent Anticoagulant and Selective Inhibitor of Factor Xa. *Thromb. Haemost.* **1994**, *71*, 314−319. Katakura, S.; Nagahara, T.; Hara, T.; Iwamoto, M. A Novel Factor Xa Inhibitor: Structure−activity Relationships and Selectivity Between Factor Xa and Thrombin. *Biochem. Biophys. Res. Commun.* **1993**, *197*, 965−972. (d) Maduskuie, T. P.; McNamara, K. J.; Ru, Y.; Knabb, R. M.; Stouten, P. F. Rational Design and Synthesis of Novel, Potent Bisphenylamidine Carboxylate Factor Xa Inhibitors. *J. Med. Chem.* **1998**, *41*, 53−62. (e) Shaw, K. J.; Guilford, W. J.; Dallas, J. L.; Koovakkat, S. K.; McCarrick, M. A.; Liang, A.; Light, D. R.; Morrissey, M. M. (*Z, Z*)-2,7-Bis(4-amidinobenzylidene)cycloheptan-1-one: Identification of a Highly Active Inhibitor of Blood Coagulation Factor Xa. *J. Med. Chem.* **1998**, *41*, 3551−3556.

(4) Whitlow, M.; Arnaiz, D.; Buckman, B. O.; Davey, D. D.; Griedel, B.; Guilford, W. J.; Koovakkat, S. K.; Liang, A.; Mohan, R.; Phillips, G. B.; Seto, M.; Shaw, K. J.; Xu, W.; Zhao, Z.; Xu, W. Z.; Light, D. R.; Morrissey, M. M. Crystallographic Analysis of Potent and Selective Factor Xa Inhibitors Complexed to Bovine Trypsin. *Acta Crystallogr.* **1999**, *D55*, 1395−1404. The coordinates have been deposited in the Brookhaven Protein Data Bank with identification number 1QB6.

(5) (a) Gullion, T.; Schaefer, J. Rotational-Echo Double-Resonance NMR. *J. Magn. Reson.* **1989**, *81*, 196−200. (b) Gullion, T.; Schaefer, J. Detection of Weak Heteronuclear Dipolar Coupling by Rotational-Echo Double-Resonance Nuclear Magnetic Resonance. *Adv. Magn. Reson.* **1989**, *13*, 57−83.

(6) Beusen, D. D.; McDowell, L. M.; Slomczynska, U.; Schaefer, J. Solid-State Nuclear Magnetic Resonance Analysis of the Conformation of an Inhibitor Bound to Thermolysin. *J. Med. Chem.* **1995**, *38*, 2742−2747.

(7) McDowell, L. M.; Schmidt, A.; Cohen, E. R.; Studelska, D. R.; Schaefer, J. Structural Constraints on the Ternary Complex of 5-Enolpyruvylshikimate-3-phosphate Synthase from Rotational-Echo Double-Resonance NMR. *J. Mol. Biol.* **1996**, *256*, 160−171.

(8) Gullion, T.; Baker, D. B.; Conradi, M. S. New Compensated Carr-Purcell Sequences. *J. Magn. Reson.* **1990**, *89*, 479−484.

(9) Bork, V.; Gullion, T.; Hing, A.; Schaefer, J. Measurement of $^{13}C-^{15}N$ Coupling by Dipolar Rotational Spin−Echo NMR. *J. Magn. Reson.* **1990**, *88*, 523−532.

(10) Merritt, M. A.; Christensen, A. M.; Kramer, K. J.; Hopkins, T. L.; Schaefer, J. Detection of Intercatechol Cross-Links in Insect Cuticle by Solid-State Carbon-13 and Nitrogen-15 NMR. *J. Am. Chem. Soc.* **1996**, *118*, 11278−11282.

(11) Garbow, J. R.; Jacob, G. S.; Stejskal, E. O.; Schaefer, J. Protein Dynamics from Chemical Shift and Dipolar Rotational Spin−Echo ^{15}N NMR. *Biochemistry* **1989**, *28*, 1362−1367.

(12) Pearlman, D. A.; Case, D. A.; Caldwell, J. W.; Ross, W. S.; Cheatham, T. E.; Ferguson, D. M.; Seibel, G. L.; Singh, U. C.; Weiner, P. K.; Kollman, P. A. AMBER 4.1; University of California: San Francisco, 1995.

(13) Ryckaert, J. P.; Ciccotti, G.; Berendsen, H. J. C. Numerical Integration of the Cartesian Equations of Motion of a System with Constraints: Molecular Dynamics of *n*-Alkanes. *J. Comput. Phys.* **1977**, *23*, 327−341.

(14) Berendsen, H. J. C.; Postma, J. P. M.; van Gunsteren, W. F.; Di Nola, A.; Haak, J. R. Molecular Dynamics with Coupling to an External Bath. *J. Chem. Phys.* **1984**, *81*, 3684−3690.

(15) Cornell, W. D.; Cieplak, P.; Bayly, C. I.; Gould, I. R.; Merz, K. M.; Ferguson, D. M.; Spellmeyer, D. C.; Fox, T.; Caldwell, J. W.; Kollman, P. A. A Second Generation Force Field for the Simulation of Proteins, Nucleic Acids, and Organic Molecules. *J. Am. Chem. Soc.* **1995**, *117*, 5179−5197.

(16) Gaussian 94 was used for the ab initio optimizations and partial charge calculations: Frisch, M. J.; Trucks, G. W.; Schlegel, H. B.; Gill, P. M. W.; Johnson, B. G.; Robb, M. A.; Cheeseman, J. R.; Keith, T.; Petersson, G. A.; Montgomery, J. A.; Raghavachari, K.; Al-Laham, M. A.; Zakrzewski, V. G.; Ortiz, J. V.; Foresman, J. B.; Cioslowski, J.; Stefanov, B. B.; Nanayakkara, A.; Challacombe, M.; Peng, C. Y.; Ayala, P. Y.; Chen, W.; Wong, M. W.;

Andres, J. L.; Replogle, E. S.; Gomperts, R.; Martin, R. L.; Fox, D. J.; Binkley, J. S.; Defrees, D. J.; Baker, J.; Stewart, J. P.; Head-Gordon, M.; Gonzalez, C.; Pople, J. A. Gaussian 94, Revision E.3; Gaussian, Inc.: Pittsburgh, PA, 1995.

(17) The phenylamidine group was assumed to have a higher affinity than the phenylamine for the P1 site. The K_i of benzylamine in trypsin is significantly higher than that of benzamidine: Markwardt, F.; Landmann, H.; Walsmann, P. Comparative Studies on the Inhibition of Trypsin, Plasmin, and Thrombin by Derivatives of Benzylamine and Benzamidine. *Eur. J. Biochem*. **1968**, *6*, 502−506. Benzamidine is known to bind in the P1 basic recognition pocket of trypsin with hydrogen bonds to the carboxylate of Asp 189, the hydroxyl of Ser 190, and the carbonyl oxygen of Gly 219: Bode, W.; Schwager, P. The refined crystal structure of bovine beta-trypsin at 1.8 Å resolution. II. Crystallographic refinement, calcium binding site, benzamidine binding site and active site at pH 7.0. *J. Mol. Biol.* **1975**, *98*, 693−717.

(18) McDowell, L. M.; Klug, C. A.; Beusen, D. D.; Schaefer, J. Ligand Geometry of the Ternary Complex of 5-Enolpyruvylshikimate-3-phosphate Synthase from Rotational-Echo Double-Resonance NMR. *Biochemistry* **1996**, *35*, 5395−5403.

(19) Goetz, J. M.; Schaefer, J. REDOR Dephasing by Multiple Spins in the Presence of Molecular Motion. *J. Magn. Reson*. **1997**, *127*, 147−154.

(20) Spellmeyer, D. C.; Wong, A. K.; Bower, M. J.; Blaney, J. M. Conformational Analysis Using Distance Geometry Methods. *J. Mol. Graph. Model.* **1997**, *15*, 18−36.

(21) Stubbs, M. T.; Huber, R.; Bode, W. *FEBS Lett.* **1995**, *375*, 103−107.

JM9900669